International Journal of Solids and Structures 46 (2009) 4054–4063

Contents lists available at ScienceDirect

International Journal of Solids and Structures

journal homepage: www.elsevier.com/locate/ijsolstr

# A macroscopic-level hybrid lattice particle modeling of mode-I crack propagation in inelastic materials with varying ductility

G. Wang [a,*], A. Al-Ostaz [a], A.H.-D. Cheng [a], P.R. Mantena [b]

[a] Department of Civil Engineering, University of Mississippi, Oxford, MS 38677-1848, USA
[b] Department of Mechanical Engineering, University of Mississippi, Oxford, MS 38677-1848, USA

ARTICLE INFO

*Article history:*
Received 5 January 2009
Received in revised form 22 June 2009
Available online 6 August 2009

*Keywords:*
Fracture mechanics
Cracks
Lattice model
Particle model
Hybrid lattice particle model
Constitutive relations

ABSTRACT

This paper presents a numerical method, known as hybrid lattice particle modeling (HLPM), for the study of mode-I crack formation and propagation in two-dimensional geometry subject to a fixed-grip condition. The HLPM combines the strength of two numerical techniques, particle model (PM) and lattice model (LM), for the purpose of solving dynamic fragmentation of solids within a various Poisson's ratio range. A Lennard-Jones-type potential is employed to describe the nonlinear dynamic interaction of each macroscopic-size particle with its nearest-neighbors. Crack initiation and propagation is investigated for materials with different Young's modulus, tensile strength and varying ductility. It is demonstrated that crack patterns and propagation closely match the anticipated physical behavior of inelastic materials. Finally, the HLPM is applied to the investigation of a functionally designed composite material of an elastic–brittle infrastructure material coated with a ductile layer for the protection of fracture propagation. The ultimate application is aimed at the retrofitting of failing infrastructure.



## 1. Introduction

Dynamic fracture is a complex and multi-scale physical phenomenon. From the microscopic point of view, fracturing is a process that material becomes separated due to the successive breakage of atomic bonds. Since the intrinsic strength properties at atomic structure level are available, molecular dynamics (MD) analysis has been the primary tool at the nano scale. Moreover, a discrete microscopic description in MD also allows defining local temperatures, potential energies, stress distributions and other quantities. These parameters present a precise physical meaning and are the key to understanding fracture. Thus, MD can provide a more fundamental insight into material behavior and its interactions. However, although MD simulation has benefitted from the rapid development of computing power and is becoming increasingly popular, the present state of computer technology is still far from being able to meet the demands of the macroscopic tasks. For example, we currently still cannot simulate a $1 \times 1 \times 1$ cm$^3$ cubic copper body at atomic level because the body consists of $10^{24}$ copper atoms, a number so large that no computer in the world can handle it. The second difficulty is its incapability in reaching the practical time scales. For instance, the laboratory dynamic fracture experiments generally last in microseconds (1 ms = $10^{-6}$ s), while the MD model time steps are typically in the nano ($10^{-9}$) or pico ($10^{-12}$) second range. As such, the MD is limited to a narrow range of solving nano- to micrometer scale problems. For this reason, a numerical tool for the modeling of dynamic fracture at macroscopic level is needed.

To successfully solve the dynamic fracture of materials at macroscopic level, it is critical if the model can deal with the uncertain evaluation of material body – large deformation or even fragmentation at a very high rate. In the other word, a successful dynamic fracture solver lies in an efficient solution of "re-meshing" in computation. The current numerical approaches for dynamic fracture simulation at macroscopic level can be generally classified into two categories – a continuum mechanics based approach (CMBA for short) and a discrete element based approach (DEBA for short). In brief, the CMBA is built up regarding the material body as one continuum media. Numerically, such models, e.g., finite element method (FEM), use space-averaging to set up constitutive equations within each element. In contrast, the DEBA shares a common concept of "discrete material", and the constitutive equations are assigned to define the interaction among the discrete neighbors. Examining the state-of-the-art of the research, we conclude that FEM, the most widely used CMBA, has difficulty in solving dynamic fracture problems, particularly in simulating collapse/fragmentation of materials under extreme loadings. Although FEM has constantly been developed to meet such requirements and several re-meshing techniques, i.e., Lagrange, Euler and Arbitrary Lagrange Euler, have been well established, fragmentation of materials is still unable to be well simulated. In contrast, the discrete element

* Corresponding author. Tel.: +1 662 915 5369; fax: +1 662 915 5523.
*E-mail address:* gewang@olemiss.edu (G. Wang).

0020-7683/$ - see front matter © 2009 Elsevier Ltd. All rights reserved.
doi:10.1016/j.ijsolstr.2009.08.001

based, or meshless, approach is robust in solving the re-meshing. Fig. 1 illustrates a material impact simulation by using FEM accounting for different re-meshing skills and by a meshless model, smoothed particle hydrodynamics (SPH) (Quan et al., 2003). It is clearly shown that the DEBA is superior to the CMBA in solving the fragmentation of materials; hence, it attracts increasing interests.

Particle modeling (PM) is the one among a number of the branches of DEBAs (Cundall, 1988; Meguro and Tagel-Din, 2000; Oñate et al., 2004; Monaghan, 2005). The PM was originally proposed by Greenspan (1997). In essence, PM, treating each computation cell as a particle with the mass lumped to its center, can be regarded as an upscale MD, but applied to large length scale and time scale problems. However, Greenspan (1997) developed such model with in mind more fluid modeling than solid modeling. As a consequence, there was no direct linkage to the solid material properties, making PM an empirical model without demonstrated validation with real engineering problems.

Lattice model (LM), on the other hand, has a long history of success in modeling micromechanics solid problems (Askar, 1985; Noor, 1988; Ostoja-Starzewski, 2002, 2007; Bolander and Sukumar, 2005; Berton and Bolander, 2006). The LM, however, does not have the flexibility of particle models, in which the particles can be subjected to very large deformation (displacement) and even fragmentation. Such limitation of LM comes from a fact of that it adopts a conjugate gradient method with respect to minimizing the total potential energy stored in all spring bonds to determine the displacement. Consequently, only one bond is allowed to fracture during each computational cycle (Alkhateb et al., 2009). Hence, the LM has so far been restricted to small motions. It is basically a *static/quasi-static* model, and does not model the *dynamic* fracture process. In Table 1, the strengths and weaknesses of the traditional LM and PM are summarized and compared.

To extend the capability of both LM and PM, and to allow the modeling of dynamic fracture and fragmentation of materials caused by impact, blasting and other extreme loadings, a hybrid lattice particle model (HLPM) has been developed based on Wang and Ostoja-Starzewski's PM (2005). As demonstrated in Table 1, the HLPM has been proposed that combines the strengths of LM and PM (Wang et al., 2009), in which the interaction potential can be described by employing either linear (quadratic) or nonlinear (Lennard-Jones or polynomial) type to the axial/angular linkage. The defined spring constants are then mapped into lattice system, which are in turn matched with the material's continuum-level elastic moduli and strength. The HLPM can readily simulate dynamic behaviors of materials at macro-scales with a varying Poisson's ratio range (Wang et al., 2009). The principle of HLPM can be described as follows: the particle–particle interaction is derived from lattice modeling (LM) theory whereas the computational scheme follows particle modeling (PM) technique. Once the translational strength is exceeded, the spring is broken and a fracture is created.

The advantages of HLPM over the existing discrete element based methods can be summarized as follows:

(1) Easy for the determination of input parameters. Four conservative/equivalent rules (mass, potential energy, Young's modulus and tensile/compression strength) are required to determine the material properties for the input datasheet.
(2) Easy for implementation. Since the physical size of each particle is ignored other than its equivalent mass, the algorithm of coding a HLPM computation is fairly easy.

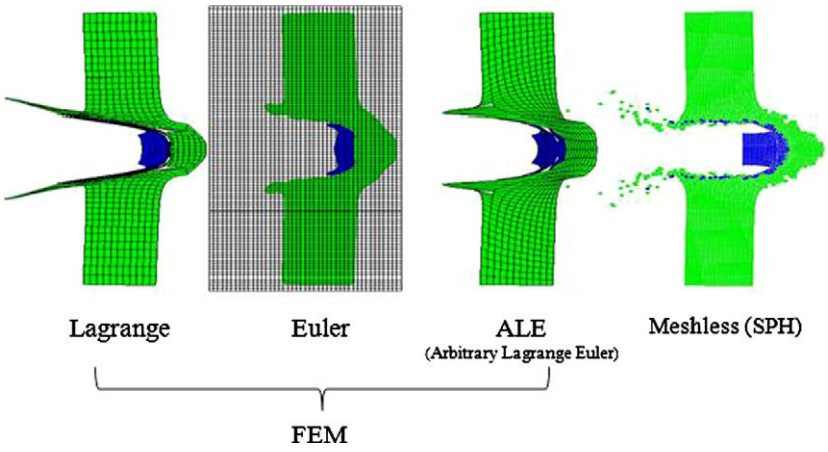


**Fig. 1.** A material impact simulation by using FEM accounting for different re-meshing skills, Lagrange, Euler and Arbitrary Lagrange Euler (ALE), and smoothed particle hydrodynamics (SPH) (Quan et al., 2003).

**Table 1**
Comparison of the lattice model (LM), the particle model (PM), and the hybrid lattice particle model (HLPM).

| | Lattice model (LM) | Particle model (PM) | Hybrid lattice particle model (HLPM) |
|---|---|---|---|
| Particle interaction | Spring (axial/angular), beam, etc. | Lennard-Jones potential (axial only) | Spring (axial/angular) mimicking the Lennard-Jones potential |
| Interaction neighborhood | Not limited to nearest neighbor | Nearest neighbor only | Not limited to nearest neighbor |
| Mesh system | Small deformation | Large deformation | Large deformation |
| Poisson's ratio | Flexible | Fixed | Flexible |
| Time process | Static | Dynamic based on Newton's second law | Dynamic based on Newton's second law |
| Force–displacement relation | Displacement (strain) interpreted from force (stress) | Force interpreted from displacement (distance between particles) | Force interpreted from displacement (distance between particles) |

A successful HLPM simulation have been achieved in predicting the fracture pattern of an epoxy plate with randomly distributed holes in tension, shown in Fig. 2(a) and (b) (Ostoja-Starzewski and Wang, 2006). Here is pointed out that, in the simulation, the Poisson's ratio of epoxy was set to 1/3. This is a special case of HLPM in which all the angular interactions are absent (Wang et al., 2009). As the figure illustrates, compared with the experimental observation, HLPM prediction of crack pattern seems more accurate than that of the FEM solution. Moreover, two successful qualitative comparisons currently have been completed with the dynamic failure experiments of polymeric material (nylon-6,6 and vinyl ester) indentation, shown in Fig. 3(a) and (b) (Wang et al., 2008a) and Fig. 4(a) and (b) (Wang, 2009), respectively.

After gaining the confidence of HLPM from the above-mentioned fracture study cases, in this paper, we step forward to investigate the modeling capability of the HLPM on the initiation and propagation of mode-I fracture in inelastic materials with different ductility employing a fixed-grip condition. As the mechanism for fracture formation and propagation in the lattice and the particle model is very different from that of the continuum mechanics based fracture mechanics model, it is not clear that the physical phenomenon of stable and unstable fracture growth can be correctly predicted. In short, the continuum model uses the stress intensity factor and energy release rate concepts for fracture creation and propagation; while the discrete HLPM uses the tensile/compression strength between bonds and the first principle based dynamic interaction among the particles. To have confidence in these models for simulating dynamic fracture problems, both numerical models need to be tested and validated.

In what follows, we first briefly introduce the HLPM algorithm. It is then applied to several two-dimensional dynamic fracture problems. Particularly, the stable and unstable fracture growth corresponding to the inelastic materials with varying ductility can be faithfully reproduced, using only the physically interpreted Lennard-Jones-type potential constants. Then, the HLPM is applied to the investigation of a functionally designed composite material of an elastic–brittle infrastructure material coated with a ductile layer for the protection of fracture propagation. The ultimate application is aimed at the retrofitting of failing infrastructure.

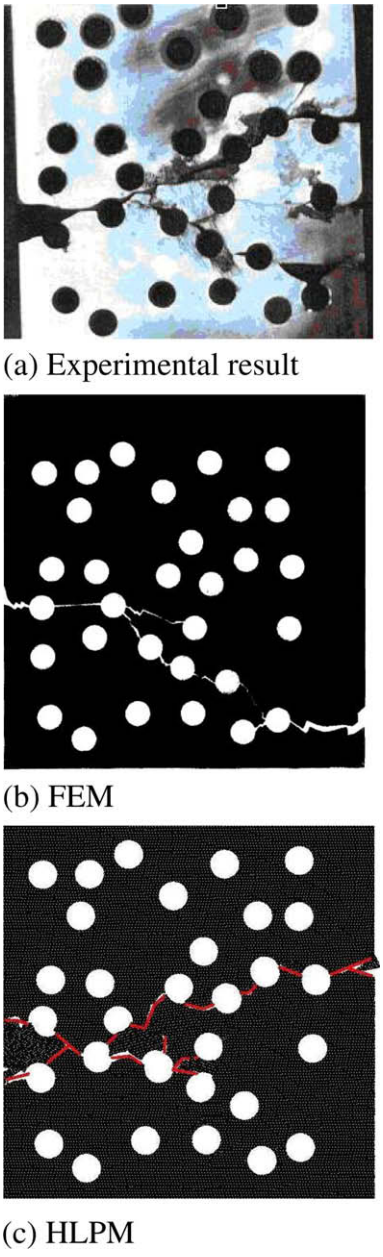


**Fig. 2.** Experimental and modeling results of epoxy in tension: (a) experiment (Al-Ostaz and Jasiuk, 1997) and (b) HLPM simulation (Ostoja-Starzewski and Wang, 2006).

## 2. Model description

The hybrid lattice particle model (HLPM) – also called lattice particle simulation, discrete modeling, or quasi-molecular modeling – is a dynamic simulation model that typically uses a relatively small number of particles of macroscopic sizes, representing solid and/or fluid mass. The particles' location and velocity evolves according to the laws of Newtonian mechanics. The axial force interaction between particles is modeled after Wang and Ostoja-Starzewski (2005) (reason: conventional LM only works for linear considerations), which is matched up with the Young's modulus and tensile strength of the material as well as energy and mass. The angular force interaction between the adjacent sides of each particle is after Wang et al. (2009). In principle, the distance of particle spacing can decrease to a few angstroms; in that case we recover a molecular dynamics like model. Hence the HLPM is fairly flexible in modeling physical phenomena of all sizes, limited only by the number of particles needed in the modeling (computational power).

The theoretical derivation of non-thermal-based HLPM can be briefly reviewed as follows.

In HLPM, the nonlinear axial interaction force between neighboring (quasi-) particles, $F$, can alternatively take the same form as in MD:

$$F = -\frac{G}{r^p} + \frac{H}{r^q} \tag{1}$$

Here $G$, $H$, $p$ and $q$ are positive constants, and $q > p \geqslant 1$ to obtain the repulsive effect that is necessarily (much) stronger than the attractive one, $r$ being the distance between two particles.

Ashby and Jones (1980) presented a simple method to evaluate continuum-type Young's modulus $E$ and tensile stress $\sigma(r)$ of the material from $F(r)$, namely

$$E = \frac{S_0}{r_0} \tag{2}$$

and

$$\sigma(r) = NF(r) \tag{3}$$

where $S_0 = (dF/dr)_{r=r_0}$, and $r_0$ is the equilibrium spacing between contiguous particles. $N$ is the number of bonds/unit area, equal to $1/r_0^2$. Tensile strength, $\sigma_{TS}$, results when $dF(r_d)/dr = 0$, that yields,

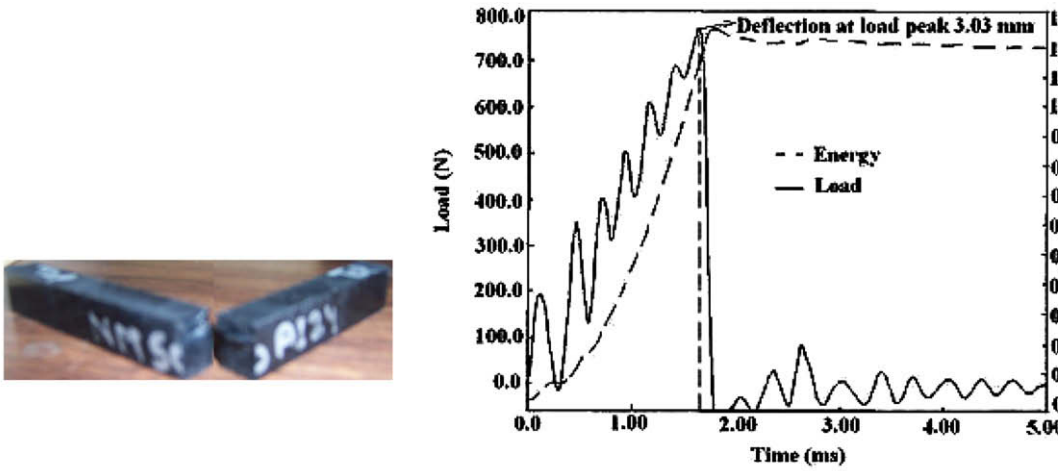


(a) Experimental results

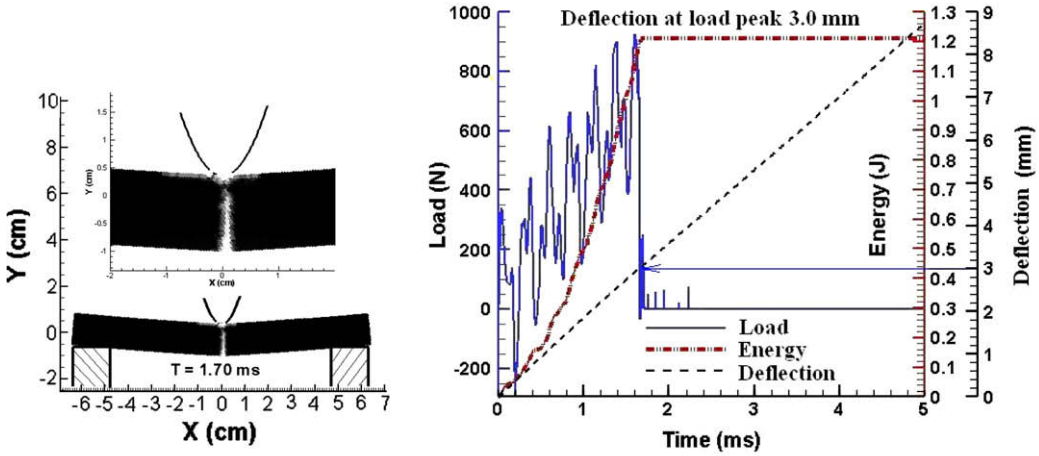


(b) HLPM results

**Fig. 3.** The study of the failure of nylon-6,6 due to the impact of a rigid indenter (a) experimental results; (b) HLPM results. Maximum drop velocity of indenter is 1.87 m/s (Wang et al., 2008b).

$$\sigma_{TS} = NF(r_d) \tag{4}$$

Note that Eq. (2) has been demonstrated to be completely consistent with LM derivation (Wang et al., 2009).

Just as in MD, the nonlinear dynamical equation of motion for each particle $P_i$ of the PM system is given by

$$m_i \frac{d^2\vec{r}_i}{dt^2} = \sum_{j=1}^{K} \left[ \left( -\frac{G_i}{r_{ij}^p} + \frac{H_i}{r_{ij}^q} \right) \frac{\vec{r}_{ji}}{r_{ij}} \right], \quad i \neq j \tag{5}$$

where $m_i$ and $\vec{r}_{ji}$ are mass of $P_i$ and the vector from $P_j$ to $P_i$; $K$ is the total number of ambient particles interacting with particle $i$. In the present study, only the nearest neighboring particles are considered which is addressed by Wang and Ostoja-Starzewski (2005).

The derivation of four parameters in Eq. (1) from MD structures is conducted on a cubic body with volume $V(=A\times B\times C)$ (Wang and Ostoja-Starzewski, 2005). A face-centered cubic (fcc) lattice for both atomic and quasi-particle structures is chosen. If $p$, $q$ and $r_0$ are given, then, by conditions of mass and energy conservation, $G$ and $H$ can be derived. Consequently, Young's modulus is evaluated by Eq. (2) and tensile strength by Eq. (4). To represent an expected material property, we would have to do many sets of testing until a unique $(p,q)$ is found to match both Young's modulus and tensile strength of the material. The complete derivation process is described below.

First, for the atomic structure (MD model), we have:

Interaction potential energy (ergs):

$$\phi_a = \left( \frac{G_a r^{1-p_a}}{1-p_a} + \frac{H_a r^{1-q_a}}{1-q_a} \right) \times 10^{-8} \tag{6}$$

Young's modulus (GPa) is obtained from Eq. (2) and tensile strength (MPa) from Eq. (4).

Total number of atoms in $A\times B\times C$ cubic material body:

$$N^* = \left( \frac{A\times 10^8}{r_a} + 1 \right) \times \left( \frac{B\times 10^8}{r_a \sin 60^0} + 1 \right) \times \left( \frac{C\times 10^8}{r_a\sqrt{6}/3} + 1 \right) \tag{7}$$

In Eqs. (6) and (7), $r_a$ is equilibrium position of the simulated material in atomic structure, and $p_a, q_a$ are the exponential parameters in atomic structure. Note that, for a Lennard-Jones interaction case, $p_a = 7$ and $q_a = 13$.

Next, for the quasi-particle structure (PM model), we have interaction force (dynes) as in Eq. (1).

Interaction potential energy (ergs):

$$\phi = \frac{G_r^{1-p}}{1-p} + \frac{H_r^{1-q}}{1-q}, \text{ for } p>1; \quad \phi = G\ln r + \frac{H_r^{1-q}}{1-q}, \text{ for } p=1 \tag{8}$$

Total number of quasi-particles in PM system:

$$N = i_{max} \times j_{max} \times k_{max} \tag{9}$$

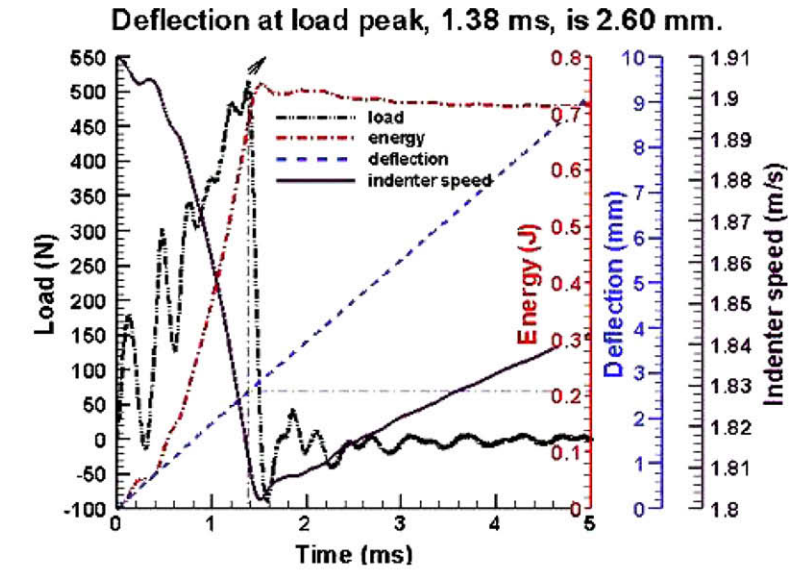


(a) Experimental observation

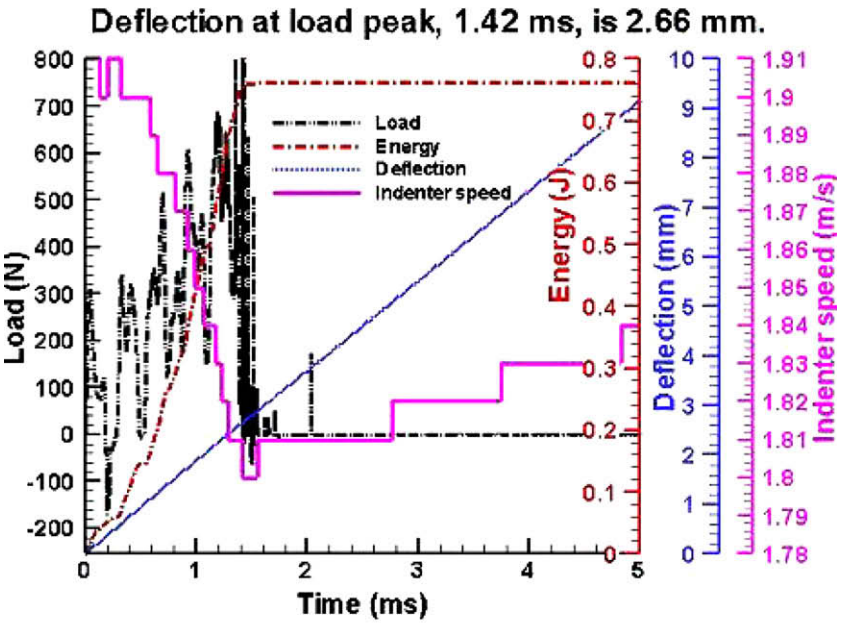


(b) HLPM simulation

**Fig. 4.** Comparison of HLPM result with the according experimental observation of the failure of vinyl ester due to the impact of a rigid indenter: (a) experimental observation and (b) HLPM simulation. Maximum drop velocity of indenter is 1.91 m/s.

We now postulate the equivalence of MD and PM models. From the mass conservation, we calculate the mass of each quasi-particle $m$ based on atomic mass $m_a$:

$$m = N^* \times m_a / N \tag{10}$$

From the energy conservation, we have:

$$(N \times \phi)_{r=r_0} = (N^* \times \phi_a)_{r=r_a} \tag{11}$$

Under the requirement:

$$F(r_0) = 0 \tag{12}$$

From Eqs. (11) and (12), we now derive Young's modulus $E$:

For $p = 1$:

$$G = H r_o^{1-q}, \quad H = \frac{(N^* \times \phi_a)_{r=r_a}(1-q)}{N(1-q) r_0^{1-q} \ln r_0 - r_0^{1-q}}, \qquad E = -G r_0^{-3} + q H r_0^{-q-2} \tag{13}$$

for $p > 1$:

$$G = H r_o^{1-q}, \quad H = \frac{(N^* \times \phi_a)_{r=r_a}(1-p)(1-q)}{N(p-q)} r_0^{q-1}, \qquad E = -pG r_0^{-p-2} + q H r_0^{-q-2} \tag{14}$$

Similarly, tensile strength can be obtained under $dF(r_d)/dr = 0$. Evidently, the four parameters $(p, q)$, $r_0$ and $V$ affect $E$ and $\sigma_{TS}$.

We have established the equations for $G$, $H$, $p$ and $q$, and carried out a parametric study to find the differing effects on $p$, $q$, $V$ and $r_0$

(Wang and Ostoja-Starzewski, 2005). Herein, we summarize the obtained rules as follows:

(i) The larger the values of $(p,q)$ are adopted, the larger is $E$ generated. This is typically associated with the material becoming more brittle than ductile, albeit there is a range of toughness to choose from. Also, with $E$ going up, there is a fragmentation into a larger number of pieces.
(ii) In the case of $p=1$, the larger $r_0$ spacing is adopted, the higher is Young's modulus of the PM material. On the contrary, in the special case of $p\neq 1$, there is an opposite trend. In any case, this increase or decrease does not change very much.
(iii) In the case of $p\neq 1$, while keeping the volume fixed, an increase of $r_0$ produces a decrease of Young's modulus. The situation is again opposite in the case of $p=1$.
(iv) A uniform augmentation of volume $V$ by dilation in all three coordinate directions $(xyz)$, at any $(p,q)$ combination, results in Young's modulus increasing first strongly and then leveling off.

For elastic–brittle materials, a general format of linear dynamical equation is often employed for axial springs (Wang et al., 2008a),

$$F=\begin{cases}-S_0(r-r_0) & \text{for } r_c\leqslant r\leqslant r_t\\ 0 & \text{otherwise}\end{cases} \tag{15}$$

with $r$ being the distance between two particles, the axial stiffness $S_0=E\cdot r_0$ by Eq. (2), $E$ the Young modulus and $r_0$ the equilibrium spacing between the contiguous particles.

In Eq. (15), $r_c$ and $r_t$ are the fracture positions applied for compression and tension, respectively, which in practice need to be empirically determined.

An analogous angular spring interaction scheme to Eq. (15) yields,

$$F_\beta=\begin{cases}-S_\varphi(\varphi-\varphi_0) & \text{for } \varphi_c\leqslant\varphi\leqslant\varphi_t\\ 0 & \text{otherwise}\end{cases} \tag{16}$$

with $\varphi_0$ the equilibrium angle between adjacent particles, and ce:italic>/ce:italic> the angular displacement. $\varphi_c$ and $\varphi_t$ in Eq. (16) are the angular fracture coefficients applied for compression and tension, respectively, which are also needed to be determined by empirical tests.

The angular stiffness $S_\varphi$ in Eq. (16) is after Wang et al. (2009),

$$S_\varphi=\frac{\sqrt{3}(1-3\nu)Er_0^2}{18(1-\nu^2)} \tag{17}$$

with $\nu$ the Poisson's ratio.

The leapfrog method, with second-order accuracy, is employed in the HLPM simulations. The leapfrog formulas relating position, velocity and acceleration for particles $P_i$ $(i=1,2,\ldots,N)$ (Greenspan, 1997) are

$$\vec{V}_{i,1/2}=\vec{V}_{i,0}+\frac{(\Delta t)}{2}\vec{a}_{i,0}\quad\text{(starter formula)} \tag{18}$$

$$\vec{V}_{i,k+1/2}=\vec{V}_{i,k-1/2}+(\Delta t)\vec{a}_{i,k},\quad k=1,2,3,\ldots \tag{19}$$

$$\vec{r}_{i,k+1}=\vec{r}_{i,k}+(\Delta t)\vec{V}_{i,k+1/2},\quad k=0,1,2,\ldots \tag{20}$$

where $\vec{V}_{i,k}$, $\vec{a}_{i,k}$ and $\vec{r}_{i,k}$ are the velocity, acceleration and position vectors of particle $i$ at time $t_k=k\Delta t$, $\Delta t$ is the time step. $\vec{V}_{i,k+1/2}$ stands for the velocity of particle $i$ at time $t_k=(k+1/2)\Delta t$, and so on. Notably, the leapfrog method is of second-order accuracy: $O((\Delta t)^2)$.

The safe time step is after the derivation result by Hockney and Eastwood (1999):

$$\Omega\Delta t\ll 2,\quad \Omega=\left(\frac{1}{m}\left|\frac{dF}{dr}\right|_{\max}\right)^{1/2} \tag{21}$$

To readily describe the breakage effect on material, we define a concept of fracture density (Wang et al., 2008b). By this definition, the local fracture density of particle $i$, $f_{i_{\text{den.}}}$, is equal to the ratio of its current number of broken bonds, $N_{b_i}$ to its original number of bonds, $N_{o_i}$, i.e.,

$$f_{i_{\text{den.}}}=\frac{N_{b_i}}{N_{o_i}} \tag{22}$$

It is clearly seen that a big $f_{i_{\text{den.}}}$ value indicates a severe failure locally occurring at $i$.

Note that different failure criterion for inelastic and elastic materials shown in Eqs. (1) and (15) are employed as a cut-off for the axial interaction force. For instance, necking position, $dF(r_d)/dr=0$, is adopted for inelastic material expressed in Eq. (1); for elastic–brittle material expressed in Eq. (15), using tensile stress, $\sigma_{\text{TS}}$, from Hooke's law, we determine the failure strain $\varepsilon_{\max}$

$$\frac{r_{\max}-r_0}{r_0}=\varepsilon_{\max}=\frac{\sigma_{\text{TS}}}{E} \tag{23}$$

and the displacement threshold for fracture to occur, $r_{\max}$.

Angular failure criterion follows the analogous scheme to Eq. (22) whereas shear strength is accounted for.

## 3. Results

In this section we first report a preliminary HLPM study of crack formation and propagation in a 2D, end-notched plate, subjected to a constant uniaxial tensile loading. The computational domain is a 2D $3.46\,\text{cm}\times 64\,\text{cm}$ plate with an initial particle spacing $r_0=0.2$ cm, and a crack of length $l_0=0.8$ cm at the very left end; see Fig. 5. A fixed-grip condition with a constant vertical stretching rate $V=40.0$ cm/s is applied to the two ends in the $Y$ direction. We assign $(p,q)=(3,5),(5,10)$ and $(7,14)$ in Eq. (1) for three different inelastic materials. Table 2 illustrates the physical outcomes by using these three $(p,q)$ values under equilibrium lattice spacing $r_0=0.2$ cm. Fig. 6 displays the according interaction force profile vs. the three above-employed $(p,q)$ values. For simplicity, we assume the Poisson's ratios of the three materials are all equal to 1/3. Consequently, the angular spring effect is absent (Wang et al., 2009).

Table 2 illustrates that with the increase of $(p,q)$, the Young's modulus and tensile strength values of the resultant material also increase. So does the necking position of the interaction force pro-

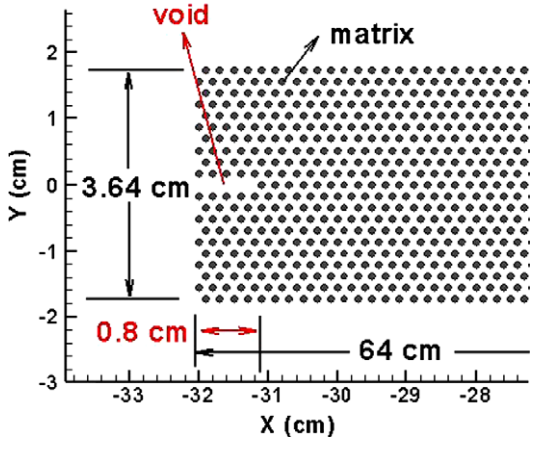


**Fig. 5.** Schematic of computational domain setup for a 2D plate with an initial crack. Particle spacing $r_0=0.2$ cm.

**Table 2**
Physical outcomes with $(p,q) = (3,5), (5,10)$ and $(7,14)$ under equilibrium lattice spacing $r_0 = 0.2$ cm.

| $(p,q)$ | (3,5) | (5,10) | (7,14) |
|---|---|---|---|
| $G$ | $2.473 \times 10^7$ | $1.781 \times 10^6$ | $1.102 \times 10^5$ |
| $H$ | $9.892 \times 10^5$ | $5.698 \times 10^2$ | 1.411 |
| $E$ (GPa) | 15.457 | 69.557 | 150.706 |
| $\sigma_{TS}$ (MN/m$^2$) | 86.205 | 263.570 | 441.534 |
| Necking position | $1.29 \cdot r_0$ | $1.15 \cdot r_0$ | $1.11 \cdot r_0$ |

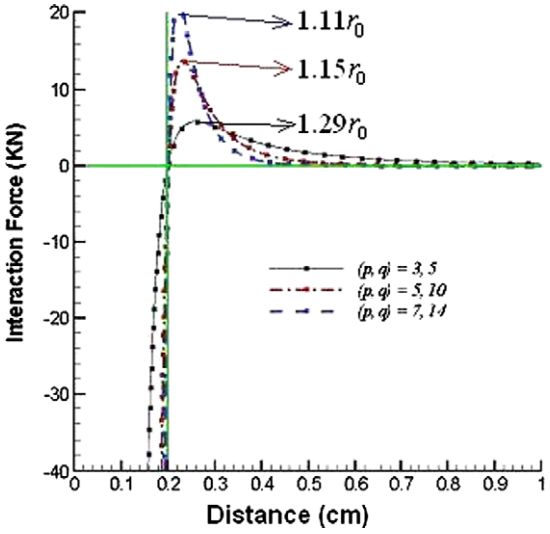


**Fig. 6.** Interaction force of HLPM under $r_0 = 0.2$ cm, with $(p,q) = (3,5), (5,10)$ and $(7,14)$.

file shown in Fig. 6 as well as in Table 2. This indicates that the material with big $(p,q)$ behave in low ductility and vice versa. Among these three materials indicated by the associated $(p,q)$, if we label $(p,q) = (3,5)$ as a ductile one (with high ductility), then $(p,q) = (5,10)$ and $(7,14)$ are in order labeled comparatively more brittle ones (with low ductility).

Fig. 7 shows the different stages of the crack propagation, from the initial crack formation, to the propagation, and to the final crack pattern, for the material, $(p,q) = (3,5)$, with high ductility. Figs. 8 and 9 show, respectively, the similar stages for $(p,q) = (5,10), (7,14)$, with comparatively low ductility.

Comparing Figs. 7–9, we observe:

(i) Crack develops sooner and propagates faster in material with low ductility (Fig. 8) than in material with high ductility (Fig. 7).
(ii) For low-ductility material, crack propagation tends to behave in an unstable manner by taking a zigzag path with varying speed (Figs. 8 and 9(c)). For high-ductility material, we observe a largely steady state growth with a smooth path (Fig. 7(c)).

Fig. 10 shows a zoomed section of the plate during the propagation stage, for comparatively the most brittle case among the three ones with $(p,q) = (7,14)$. It is observed that there are micro-cracks forming in a region ahead of the main crack (marked by circle and ellipses), attracting the main crack toward it, thus creating a zigzag path. This phenomenon was indeed observed in brittle-like materials, and not in ductile-like materials (Abraham, 1997). Fracture of this type is called a brittle fracture. We observe that the HLPM can truthfully capture this delicate phenomenon by simply prescribing a Lennard-Jones-type potential that corresponds to brittle materials. Hence the HLPM can serve an important function of correctly modeling the time dependent ductile and brittle crack propagation.

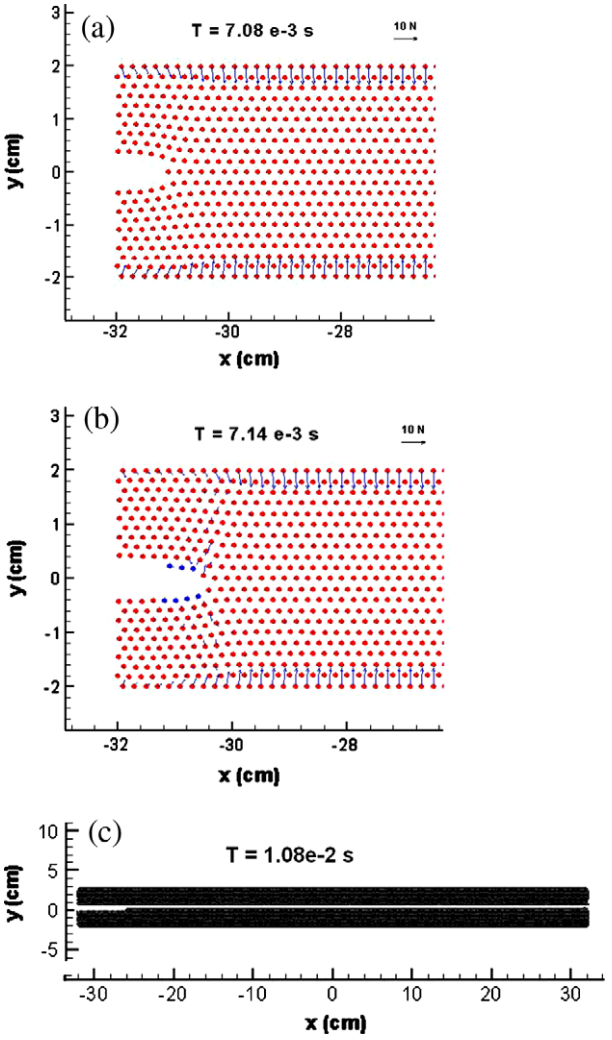


**Fig. 7.** Time-dependent fracture propagation of 2D plate with an initial crack, for ductile, $(p,q) = (5,10)$. Stretching rate = 40 cm/s. (a) $t = 7.08$ ms, (b) $t = 7.14$ ms, and (c) final crack pattern.

Next, we apply the HLPM to the investigation of some structure retrofitting ideas. First, we investigate an elastic–brittle beam subject to a point load at mid-span, with the two ends supported with permission of horizontal movement. The load is actually applied as a downward displacement at the constant rate of 50 cm/s. The two-dimensional beam is of the dimension 12.7 cm in length and 1.27 in thickness, with material properties corresponding to Young's modulus 3.0 GPa, and tensile strength 60 MPa. The dynamic interaction follows linear elastic formulas as described in Eq. (15). In Fig. 10, we present the deformation of the beam at $t = 5.6$ ms. We observe that the failure happens in the form of a zigzag fracture below the point load. The HLPM simulated crack pattern seems to agree well with the similar simulation by Cusatis and Cedolin (2006).

To investigate the retrofitting schemes, we protect the main structure as shown in Fig. 11 by a high-ductility material either on top, or at bottom of the beam, as shown in Fig. 12(a) and (b). The high-ductility material is characterized by $(p,q) = (3,5)$, which corresponds to $(E, \sigma_{TS}) = (15.5\ \text{GPa}, 86.2\ \text{MPa})$, and a necking position equal to $r_d = 1.29 r_0$, see Fig. 5. The thickness of this ductile material is 0.3 cm. Applying the same loading condition, we demonstrate the result of simulation in Fig. 13(a) and (b).

Fig. 13(a) and (b) shows the result with the retrofitted layer on the top and at the bottom, at $t = 5.6$ ms. From Fig. 13(a), we

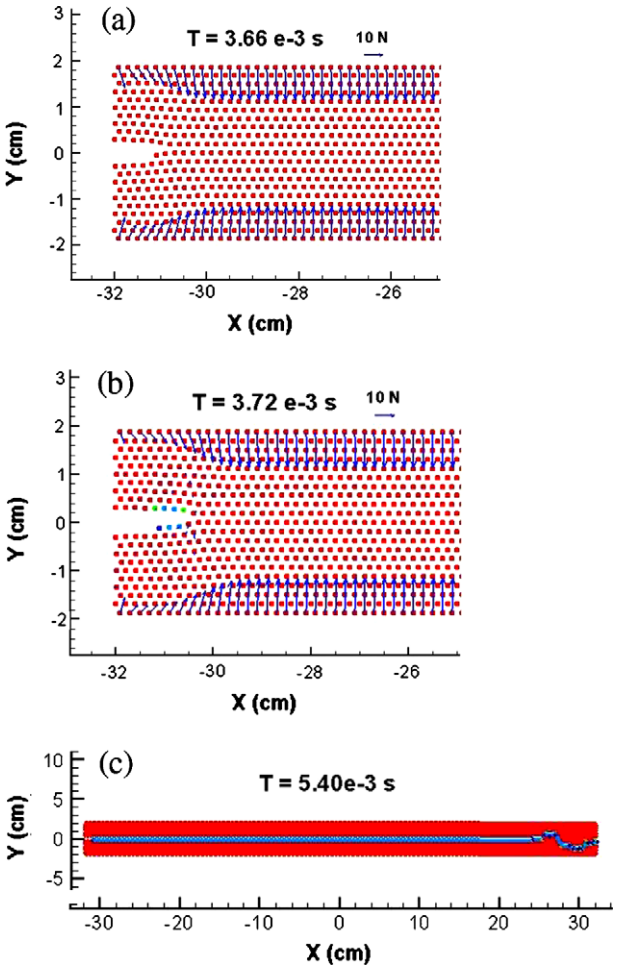


**Fig. 8.** Time-dependent fracture propagation of 2D plate with an initial crack, for ductile, $(p, q) = (5, 10)$. Stretching rate = 40 cm/s. (a) $t = 3.66$ ms, (b) $t = 3.72$ ms, and (c) final crack pattern.

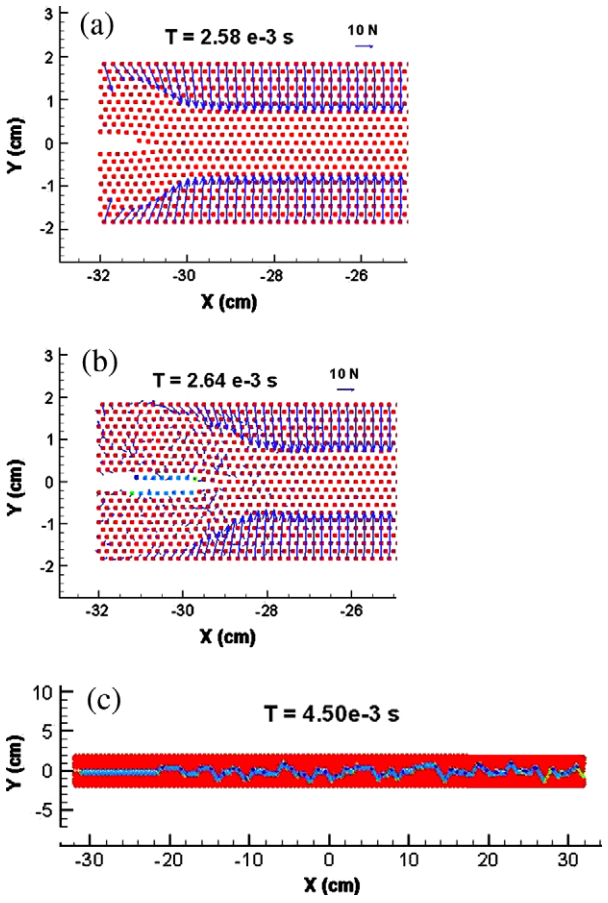


**Fig. 9.** Time-dependent fracture propagation of 2D plate with an initial crack, for brittle material, $(p, q) = (7, 14)$. Stretching rate = 40 cm/s. (a) $t = 2.58$ ms, (b) $t = 2.64$ ms, and (c) final crack pattern.

observe that the vertical crack propagates upward toward the retrofitted layer, and is arrested without penetration. At the same time, the material starts to delaminate with interfacial crack propagating along the material interface; from Fig. 13(b), we observe an extended damaged area, in the form of a wedge, underneath the load, and also some delamination along the material interface. Viewing the two retrofitted simulation results in Fig. 13(a) and (b), we see that the infrastructure is fractured in each case under the action of the point-load; however, the entire integral structure is well sustained. Comparing the two retrofitting schemes, from the resultant minimum deflection in the mid-top of the structure, we conclude that putting the retrofitted material at the bottom works better.

## 4. Concluding remarks

In this paper, a hybrid lattice particle modeling (HLPM) method is employed for a study of crack formation and propagation in mode-I for a 2D end-notched plate subject to a fixed grip condition of a constant vertical uniaxial tensile loading. Different inelastic material properties, in terms of Young's modulus, tensile strength and also with varying ductility, are accounted for with the plate. From this study, the following benefits are obtained.

In the model capability aspect, the advantages of HLPM over the existing classical mechanics tools, such as finite element method (FEM), can be outlined as follows:

(1) No need for remeshing. Remishing is known as an overwhelming challenge for FEM whereas HLPM does not at all. In HLPM, fracture is created when a bond (spring) is broken by translational force. This provides HLPM a unique power to be able to quite easily overcome a "discontinuity of material" problem.
(2) No stress intensity required. In HLPM, a bond (spring) is broken and fracture is thus resulted wherever the critical failure strain reaches.
(3) HLPM can capture more realistic crack propagation. In this paper, we see that HLPM can capture micro-cracks appearing away from the main-crack path while the fracture develops in brittle materials or metals, whereas the continuum mechanics based models rarely report.

In the aspect of the problem explored itself, it is found that crack patterns and propagation is under strong influence of material constants. The obtained results can be outlined as follows:

(1) Crack develops sooner and propagates faster in low-ductility (brittle-like) materials than in high-ductility (ductile-like) materials.
(2) Crack propagation tends to behave in an unstable manner in low-ductility materials while in a steady fashion in high-ductility materials.

Following from the above-obtained results, we then apply the HLPM to the investigation of some structure retrofitting ideas.

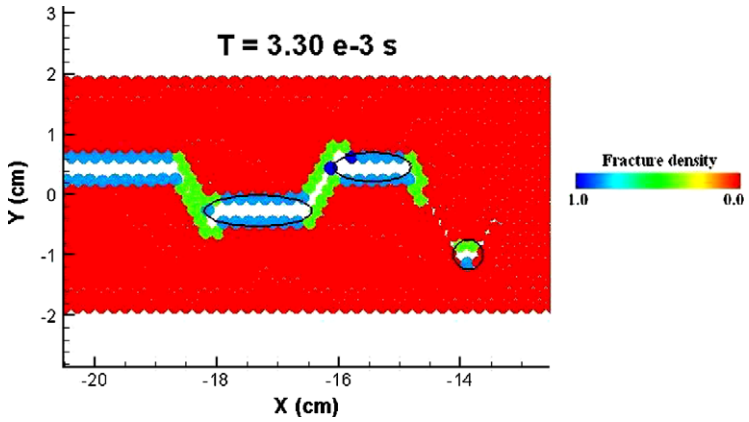


**Fig. 10.** Zooming of a HLPM simulated fracture during the propagation stage, at $t = 3.3$ ms, for brittle material, $(p, q) = (7, 14)$.

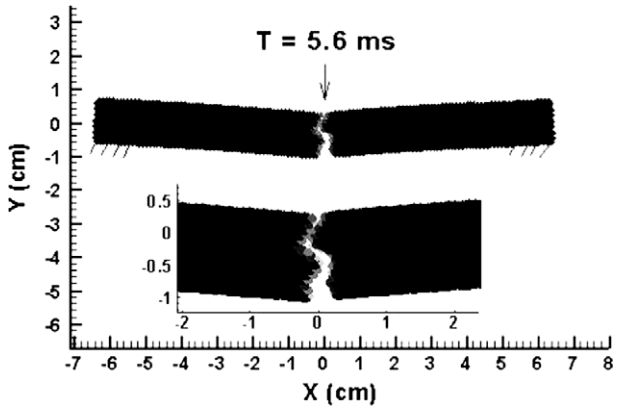


**Fig. 11.** HLPM simulation of failure of an elastic–brittle beam subject to a constant rate deformation at mid-span. Deformation rate = 50 cm/s. $t = 5.6$ ms.

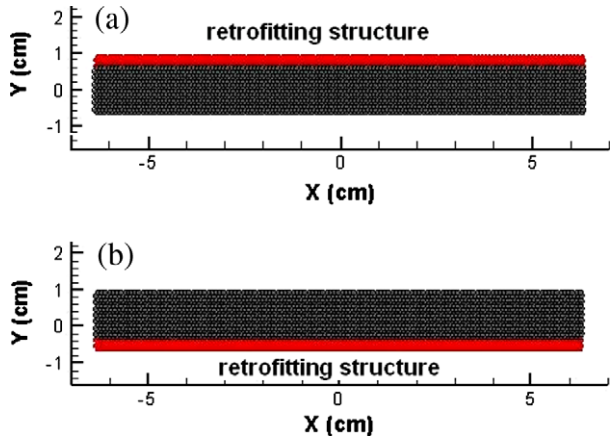


**Fig. 12.** An elastic–brittle plate coated with nonlinear ductile material: (a) retrofitted layer on the top and (b) retrofitted layer at the bottom.

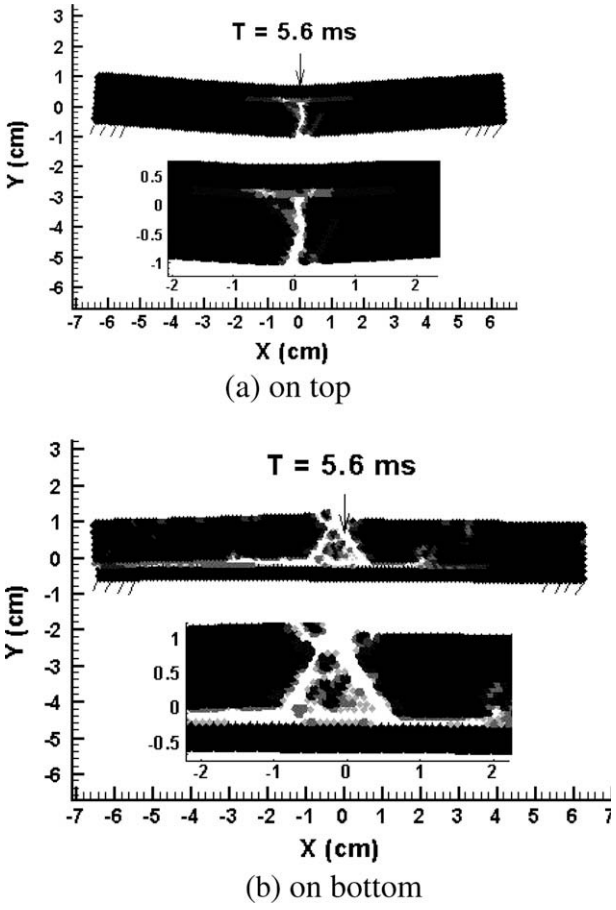


**Fig. 13.** HLPM simulated failure of an elastic–brittle plate coated with retrofitting material on top and at bottom, and subjected to a constant rate deformation at mid-span, (a) on top and (b) at bottom. Deformation rate = 50 cm/s. $t = 5.6$ ms.

We select putting a retrofitted material layer on the top and at the bottom of the infrastructure to find out a better protective effect. We conclude that integral structure with retrofitted material at the bottom produces a minimum deflection when subject to a point-load in the mid-span. The significance of this research may help guide to fabricate a high-resistance retrofitting layered structure optimally comprised of different materials. This fabricated enforcement structure is then coated to the infrastructure to effectively improve the performance of the retrofitting of failing infrastructure. In this paper, merely a preliminary simulation is attempted to identify the validation of this idea. We will report the detailed research progress of this topic in a separate paper.

## Acknowledgments

This work was partially supported by the funding received under a subcontract from the Department of Homeland Security-sponsored Southeast Region Research Initiative (SERRI) at the

Department of Energy's Oak Ridge National Laboratory, USA. The authors acknowledge the partial support for this research by ONR Grant No. N00014-07-1-1010, Office of Naval Research, Solid Mechanics Program (Dr. Yapa D.S. Rajapakse, Program Manager).

## References

Abraham, F.F., 1997. Some New Directions in Science on Computers. World Scientific, Singapore, pp. 91–113.

Alkhateb, H., Al-Ostaz, A., Alzebdeh, K.I., 2009. Developing a stochastic model to predict the strength and crack path of random composites. Composites B 40, 7–16.

Al-Ostaz, A., Jasiuk, I., 1997. Crack initiation and propagation in materials with randomly distributed holes. Engineering Fracture Mechanics 58, 395–420.

Ashby, M.F., Jones, D.R.H., 1980. Engineering Materials 1: An Introduction to Their Properties and Applications. Pergamon Press, Oxford.

Askar, A., 1985. Lattice Dynamical Foundations of Continuum Theories. World Scientific, Singapore.

Berton, S., Bolander, J.E., 2006. Crack band model of fracture in irregular lattices. Computer Methods in Applied Mechanics and Engineering 195, 7172–7181.

Berton, S., Bolander, J.E., 2006. Crack band model of fracture in irregular lattices. Computer Methods in Applied Mechanics and Engineering 195, 7172–7181.

Bolander, J.E., Sukumar, N., 2005. Irregular lattice model for quasi-static crack propagation. Physical Reviews B 71, 094106.

Cundall, P.A., 1988. Computer simulations of dense sphere assembles. Micromechanics of Granular Materials, 113–123.

Cusatis, G., Cedolin, L., 2006. Two-scale study of concrete fracturing behavior. Engineering Fracture Mechanics 74, 3–17.

Greenspan, D., 1997. Particle Modeling. Birkhäuser Publishing, Basel.

Hockney, R.W., Eastwood, J.W., 1999. Computer Simulation Using Particles. Institute of Physics Publishing.

Meguro, M., Tagel-Din, H., 2000. Applied element method for structural analysis: theory and application for linear materials. Structural Engineering/Earthquake Engineering, JSCE 17 (1), 1–14.

Monaghan, J., 2005. Smoothed particle hydrodynamics. Reports on Progress in Physics 68 (1), 1703–1759.

Noor, A.K., 1988. Continuum modeling for repetitive lattice structures. Applied Mechanics in Reviews 41 (7), 285–296.

Oñate, E., Idelsohn, S.R., Pin, F.D., Aubry, R., 2004. The particle finite element method: an overview. International Journal Computational Method 1 (2), 267–307.

Ostoja-Starzewski, M., 2002. Lattice models in micromechanics. Applied Mechanics in Reviews 55 (1), 35–60.

Ostoja-Starzewski, M., 2007. Microstructural randomness and scaling in mechanics of materials. In: Modern Mechanics and Mathematics Series. Chapman & Hall/CRC Press/Taylor & Francis, London/Boca Raton, FL/London.

Ostoja-Starzewski, M., Wang, G., 2006. Particle modeling of random crack patterns in epoxy plates. Probabilistic Engineering Mechanics 21, 267–275.

Quan, X., Birnbaum, N.K., Cowler, M.S., Gerber, B.I., Clegg, R.A., Hayhurst, C.J., 2003. Numerical simulation of structural deformation under shock and impact loads using a coupled multi-solver approach. In: 5th Asia-Pacific Conference on Shock and Impact Loads on Structures, November 12–14, Human, China.

Wang, G., 2009. Particle modeling of polymeric material indentation study. Engineering Fracture Mechanics 76, 1386–1395.

Wang, G., Ostoja-Starzewski, M., 2005. Particle modeling of dynamic fragmentation – I: theoretical considerations. Computational Materials Science 33, 429–442.

Wang, G., Al-Ostaz, A., Cheng, A.H.-D., Mantena, P.R., 2008a. Particle modeling of a polymeric material (nylon-6,6) due to the impact of a rigid indenter. Computational Materials Science 44, 449–463.

Wang, G., Radziszewski, P., Ouellet, J., 2008b. Particle modeling simulation of thermal effects on ore breakage. Computational Materials Science 43, 892–901.

Wang, G., Al-Ostaz, A., Cheng, A.H.-D., Mantena, P.R., 2009. Hybrid lattice particle modeling: theoretical considerations for a 2-D elastic spring network for dynamic fracture simulations. Computational Materials Science 44, 1126–1134.